Current count-9631

Blended tropical almond residue for fuel production: characteristics, energy benefits, and emission reduction potential

Obafemi O. Olatunji[1*], Stephen Akinlabi[2,3], Nkosinathi Madushele[1], Paul A. Adedeji[1], Matumuene J. Ndolomingo[4], Thivhani Meshack[4]

[1]Department of Mechanical Engineering Science, University of Johannesburg, South Africa
[2]Department of Mechanical and Industrial Engineering, University of Johannesburg, South Africa
[3]Department of Mechanical Engineering, Walter Sisulu University, South Africa.
[4]Department of Chemical Sciences, University of Johannesburg, South Africa

Abstract

Besides the nuts produced from almond cultivation, it also generates several million tonnes of residue that include hulls, shells, leaves, pruning, and inedible kernels which are valuable feedstocks in clean fuel production. In this article, blended tropical almond residue of two particle sizes (NT15 and NT25) were investigated. The heating, proximate and ultimate values were reported while the chemical composition of the ash was determined. Also, the pore structure and the inherent functional groups were determined for the particle sizes. The thermogravimetric analysis was also carried out to determine the thermal behaviour at different heating rate (10, 15, 30 $^{o}Cmin^{-1}$) in inert environment while the kinetic parameters were evaluated based on three non-isothermal methods (Flynn–Wall–Ozawa, Kissinger–Akahira–Sunose and distributed activation energy model). Notably, the ash content was higher in the finer particle size NT15 (1.11 %) compared to NT25 (0.87 %). Low pore surface area (1.218-0.970 m^2g^{-1}) agrees with literature values while a slight difference in pore size distribution was observed during adsorption at higher relative pressure. A representation of mixed functional groups whose wavelength falls within 527 cm^{-1}, 848 cm^{-1}, 991 cm^{-1}, 1035 cm^{-1}, 1179 cm^{-1}, 1597 cm^{-1}, 1772 cm^{-1}, 2849 cm^{-1} was observed with no significant difference between the two particle sizes. The average activation energy, E_a for NT15 and NT25 were in the range of 127.4-131 $kJmol^{-1}$ and 129-133 $kJmol^{-1}$ respectively for all the three methods, with the lowest E_a (127.4 $kJmol^{-1}$) and compensation factor, K_0 (1.29E+12 min^{-1}) obtained for the smaller particle size (NT15) based on Kissinger–Akahira–Sunose method. Finally, the energy benefits and CO_2 emission reduction potential were estimated. The highest energy potential is in USA (4.17 Mtoe) while Morocco has the highest emission reduction at 3.28 %. The information obtained from this study can be used in the scaling up of bioreactors which can further support the global clean energy drive and reduce environmental pollution.

Keywords: Blended tropical almond; Clean fuel production; CO_2 emission; Energy benefits; Particle sizes; Pore structure; Kinetic parameters.

Nomenclature

Cr_I	Crystallinity index	FTIR	Fourier Transform Infrared
E_p	Possible energy produced by using whole almond fruit (shell, and hulls)	FWO	Flynn-Wall-Ozawa
P_{NT}	Almond Production in a country (kg)	GHG	Greenhouse Gas
U_c	Unit conversion (0.000277778 WhJ^{-1})	IUPAC	Union of Pure and Applied Chemistry
f_s	Residue factor in a whole almond fruit (%)	HHV	High heating value
RH	Relative humidity	M	Moisture content (%)
T	Temperature (K)	VM	Volatile matter (%)
k	Rate constant	FC	Fixed carbon (%)
t	Time (s)	HA	High angle (degrees)
R^2	Coefficient of determination	KAS	Kissinger-Akahira-Sunose
ASTM	American Society for Testing and Materials	M	Moisture content (%)
ANOVA	Analysis of variance	Mtoe	Million tonnes of oil equivalent
DAEM	Distributed activation energy	RH	Relative humidity (%)
DTG	Differential thermogravimetry	SEM	Scanning Electron microscope
		TG	Thermogravimetric

* Contact author: *tunjifemi@gmail.com*

XRD	X-ray Diffraction
$f(\alpha)$	Mechanism function
β	Heating rate (^{0}Cmin^{-1})

1. Introduction

The global concern around climate change, environmental pollution, energy security, and fossil fuel depletion has necessitated the need for alternative energy sources so much that it has become a topic of significant focus in achieving sustainable development goals (SDGs) 2030. The 17 goals of SDGs 2030 have 169 targets, which are aimed at socio-economic and environmental sustainability (de Oliveira Neto et al., 2019). Energy is the fulcrum on which the achievement of these SDGs are hinged and most countries are depending on it since it engenders stability and economic growth of the society (Sáez-Martínez et al., 2016). Goal 7 of SDG 2030 is premised on ensuring access to affordable, reliable, sustainable and modern energy for all (UN-SDG, 2019); while goal 13 emphasises the imperative of urgent action to combat climate change (Olatunji et al., 2018; Perea-Moreno et al., 2018). To keep global warming at 1.5 °C, the net CO_2 emission will have to fall by 45% from 2010 level by 2030 (Wuebbles et al., 2017) and reach a zero level by 2050 (Olatunji et al., 2019). This has necessitated fund flow which reached $18.6 billion in 2016 from the international community in support of clean and renewable energy in the developing country (UN-SDG, 2019), also there is a devolution of financial instruments from fossil fuel exploration to encourage clean energy revolution (WorldBank, 2017). It is unlikely that fossil fuel will be able to support the energy demand of the emerging population which is growing at an exponential rate (Lizunkov et al., 2018; Smil, 2019). More so, with the current trend of carbon emission tax, the energy production from fossil fuel will be significantly affected, with a tremendous impact on profitability. Therefore, an alternative source such as bioenergy can provide opportunity towards the reduction of carbon emission tax, leading to more profitable energy production. According to International Energy Agency, IEA latest market forecast, modern bioenergy will account for the highest growth in renewable energy, RE between 2018 and 2023, this further highlights the critical role of biomass in the development of robust RE portfolio (IEA, 2018). Biomass can be converted to several energy-related products, which could be applied in electricity generation, transportation, cooking, lighting, heating, and cooling (Khiari et al., 2019; Scarlat et al., 2015). In 2016, 500 TWh of electricity was generated from biomass across the globe (Agency, 2018), this trend promises to continue as long as foremost concerns associated with bioenergy application are addressed frontally.

The source from which biofuel is derived is very vital to its sustainable exploration. The second generation of biofuel, which largely consists of waste and residue offers low lifecycle GHG emission and mitigates the global concerns around land-use change and food security with additional benefits of improving waste management and air quality. Interestingly, residues are generated across the globe from agricultural practices in large quantity and some have been valorised as a residual feedstock stream for industrial processes or domestic use. On the other hand, the third generation of biofuel broadly classified into microalgae and macroalgae, have been widely investigated (Bajpai, 2019). Although they have short harvesting cycle with higher productivity, the overall capital cost of the production is higher than the agricultural biomass residue, therefore further intensive research is ongoing in order to achieve a reasonable cost advantage (Bajpai, 2019).

Among several biomass resources which have been globally acknowledged, almond is the most cultivated tree nut (Phys.org, 2018). Between 2010-2017, global almond production was estimated at 16.4 MT; in 2017 alone 2.24 MT was produced (Fig. 1) (FAO, 2019). Almond produce residue which represents around 73 % of the total almond weight depending on the species (ABOC, 2018). These residues are often discarded as waste even though they can be used in the cosmetic, pharmaceutical and energy industries (Esfahlan et al., 2010). This discarded residue leaves an unfriendly print on the environment. On the other hand, such resources could be an addition to the existing low-cost biomass feedstock which can be applied in modern heating system. Their application can further mitigate environmental pollution and subsequently help in the reduction of CO_2 emission. More so, heat recovery from almond residue can provide substantial amount of energy which can be used in almond nut processing with less recourse to the grid since liquid and solid fuel could be produced from the conversion of this residue. Tropical almond is highly dispersed in the tropical and subtropical region with one-third of the global population and 36 % of global landmass (Encyclopedic, 2019; Togibasa et al., 2019). It has been reported as a

possible source of biodiesel with low risk of contributing to food shortages (Togibasa et al., 2019) since the major parts of the fruit are discarded as residue (ABOC, 2018).

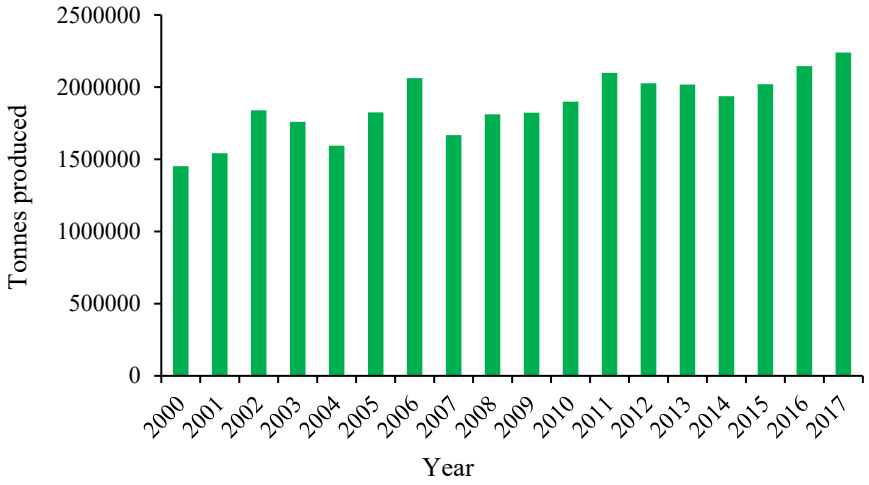

Fig. 1. Global almond production

The physicochemical properties of biomass which may be influenced by the class of biomass, climatic and soil condition, water, genetic strain, age, contaminants, pre-treatment methods, particle size and so on could affect the design of biomass conversion systems (Cai et al., 2017; Mlonka-Mędrala et al., 2019). This makes biomass to behave in some ways different from fossil fuels, which they are primed to substitute. For instance, biomass residues are heterogeneous and also of low density which sometimes makes it difficult to reduce to uniform particle sizes using standard procedures. Particle size may be an important parameter which could impact the pyrolysis of biomass (Onsree et al., 2018). An increase in particle size may lead to large temperature gradient within the particle such that the core temperature could be lesser than what is obtainable at the particle surface with a consequential effect on the product distribution. Most specifically, the previous study by Bridgeman et al. (2007) suggested that particle sizes influence the physicochemical properties of switchgrass and reed canary grass. Apart from the above mentioned, blending can influence the properties of biomass and in turn, affect fuel conversion process (Nozela et al., 2018; Wang et al., 2018). Authors are not aware of any study which have investigated the physicochemical parameters, heating value and thermal behaviour of tropical almond blend with specific emphasis on the effect of particle sizes. Base on this reason, there is a need to consider the effect of influential factors such as particle size on the properties of tropical almond.

Also, the understanding of the constituents and various properties which can impact the techno-economic suitability and enhance the development of modern and efficient conversion technologies is very important (Olatunji et al., 2020). There have been several attempts to characterize the properties of almond. Specifically, Akubude and Nwaigwe (2016) reviewed the chemical composition of edible and non-edible almond fruit while discussing their economic significance. They concluded that the entire parts of almond are rich in feedstock for bioenergy production. Queirós et al. (2019) characterized the shell of almond nuts with emphasis on the anatomical features, fractional behaviour and chemical composition while González et al. (2005) evaluated the operating conditions of the combustion process for domestic heating of almond shell, pruning and peel. Most of these efforts were focused on the chemical, proximate and heating value of biomass with few authors reporting the thermogravimetric analysis (Álvarez et al., 2016; Okoroigwe, 2015) though no reference was made to the particle size and blending in these studies. However, a comprehensive understanding of energetic properties of biomass should include the pore structure, functional groups and the crystallinity given their significance in the design of material handling equipment and storage in biofuel production. Authors are not aware of any study which have reported the pore structure, functional groups and the crystallinity for tropical almond blend.

In summary, the novelty of this study is in the investigation of the effect of particle size on the energetic properties of biomass such as the pore structure, functional groups, crystallinity, heating value, elemental composition, and thermal behaviour, and also the determination of the emission reduction potential which is the main drive for renewable energy. This study describes the relevance of almond residue as a source of renewable energy while assessing its energy characteristics as a feedstock in biofuel production . It also investigates the energy potentials

of this blended biomass residue while evaluating the impact of the variation of particle sizes on the thermal properties and kinetic parameters of the residue. Finally, the emission reduction potentials of almond in fuel production was assessed.

2. Materials and Methods

2.1 Biomass feedstock collection

The tropical almond fruits were collected at a geographical location of Modakeke ($7^0$31'35.75" N, $4^0$31'37.75" E), Osun state in April 2018. It was sundried for 7days at 33.9 ^{0}C before storing at room conditions. The resulting product was then manually cracked to remove the seeds, thus leaving behind the residue (hull and shell). The visible contaminants were carefully removed using manual method. Pulverization was done using a vibratory disk milling machine and the particles were sieved to sizes passing <250 μm (NT25) and <150 μm (NT15) sieves. The sieved tropical almond blend samples were stored in an airtight Ziplock bag and kept in the desiccator at room temperature while waiting for the characterization. The characterization of the feedstocks was based on several physicochemical parameters, which have a significant effect on the conversion pathway and fuel properties of biomass. The schematic diagram of this analysis is presented in Fig. 2.

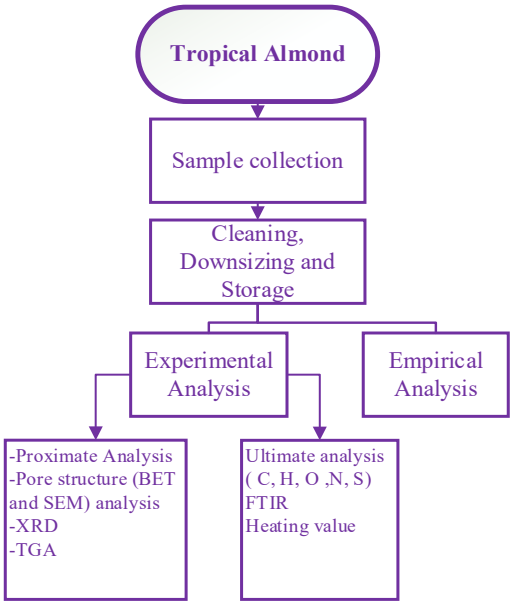

Fig. 2. Schematic diagram for Tropical almond analysis

2.2. Proximate Analysis

The proximate values of tropical almond which include M, VM, and Ash were determined according to ASTM standards (E871-82, 2013; E872-82, 2013; E1755-01, 2015) while FC was calculated by differences. All the proximate analysis were carried out under controlled temperature, time, weight, and equipment in compliance with ASTM E1757-01 (2015). Using elemental analyser, the weighted percentage of C, H, S, N were determined, and the percentage of O was calculated based on the mean differences. The chlorine content was determined according to ASTM E776-16 (2016) while the major elements in Ash were determined based on ASTM D3682-13 (2013).

2.3. Calorific Value

The heating value was experimentally determined using Cal2k Eco calorimeter (DDS, 2018). The vessel was first calibrated, then the tropical almond blend of 0.5g was used for each test. The high heating value, HHV obtained from the experiment was validated using empirical correlations that have been previously developed based on the ultimate and proximate analyses.

2.4. Brunauer Emmett and Teller (BET) Analysis

In this study, N_2-adsorption/ desorption isotherms, surface area, pore volume and pore size distribution were measured using a Micromeritics ASAP2460 surface area and porosity analyser. Before this analysis, the tropical almond blend powders were degassed with nitrogen at 90^0C for 12 h to remove the surface impurities which may lead to adsorption /desorption errors. Liquid nitrogen was used as an adsorbent to maintain an adsorption temperature of −196 °C. A sample size of 2.5g was used, while re-uptake of moisture in sample was mitigated by immediately placing a rubber stopper over the analysis tube (Leal et al., 2019). All the measurements were carried out at −196 °C and the pore volume, surface area, and sizes were calculated from the adsorption curves using Barrett–Joyner–Halenda (BJH) model (Bingwa et al., 2017) while the surface area, pore diameter were estimated using BET method (Wang et al., 2020).

2.5. X-ray Diffraction Analysis (XRD)

For the p-XRD analysis, the samples were analysed using Rigaku miniflex 600 powder diffractometer which is equipped with Cu Kα radiation source generated at 18 kW and 250 mA. High angle (HA) measurement was performed at a range of 2θ =10-50 ^{0} at a step rate of 0.4 ^{0}/min. The p-XRD pattern which was obtained was processed with Match! Version 2 software package (Crystal-Impact, 2013). The crystallinity index, Cr_I was estimated as in Eq. (1) (Segal et al., 1959; Singh et al., 2017);

$$Cr_I = \left[\frac{I_{2\theta} - I_{am}}{I_{2\theta}}\right] \times 100 \quad (1)$$

where $I_{2\theta}$ is the intensity at the HA for crystalline portion of the tropical almond blend, while I_{am} is the peak of the amorphous portion. The crystallite size, D_{002} was calculated from wide angle XRD using Debye-Scherrer equation as in Eq. (2) (Holzwarth and Gibson, 2011);

$$D_{002} = \frac{\mathrm{K}\lambda}{\mathrm{B}_{002}\, cos\theta} \quad (2)$$

where K is Scherrer constant and it is 0.9 in the case of Cu Kα radiation source, B_{002} is the full width at half maximum of the peak (FWHM) in radian, $\lambda = 0.154060nm$ is the wavelength of X-ray for Cu Kα and θ is the angle of diffraction (in radian).

2.6. Fourier Transform Infrared Spectroscopy (FTIR)

The functional group inherent in the tropical almond blend was characterized with PerkinElmer FT-IR spectrum GX specification. The 10 mg dry sample was thoroughly mixed with 200 mg KBr and compressed to form pellets. The spectra were obtained at a total scan time of 20sec within the infrared, IR range of 400-4000 cm^{-1} at 1 cm^{-1} step size.

2.7. Scanning Electron Microscopy (SEM)

The SEM analysis was performed on a Tescan Vega 3LMH scanning electron microscope with an accelerating voltage of 20kV, beam intensity of 17W/m^2 and the scanning speed of $10\mu s/pixel$. The imaging of the particle was conducted in secondary electron (SE) imaging mode.

2.8. Thermogravimetric (TG) Techniques

TG analysis was carried out using STA 7200 thermal analysis system. The thermal behaviour was studied from 25-900^{o}C at a varying heating rate of 10, 15 and 30 ^{0}C/min in an inert atmosphere (N_2) for different particle sizes. The level of pure nitrogen gas was monitored all through the experimental stages and kept at a flow rate of 20ml/min.

2.8.1. Kinetics Analyses

It is beneficial to use model-free methods since it does not force the reaction model to fit the prevailing problem. Also, the kinetic parameters derived from model-free methods do not need any presumption on reaction scheme. In this study, three non-isothermal methods; Flynn–Wall–Ozawa (FWO), Kissinger–Akahira–Sunose (KAS) and distributed activation energy model (DAEM) were evaluated in order to compare the activation energy, E_a and

the compensation (pre-exponential) factor, k_0 for the two particle sizes at varying conversion levels. These methods have been used in the recent studies on thermal degradation of different biomass feedstocks due to their simplicity and less computation intensity (Fang et al., 2020; Zou et al., 2019). FWO can accurately estimate the reaction rates and the mechanism of biomass combustion by avoiding errors and deficiencies of conventional analytical techniques while KAS technique involves integral approach to determine the kinetics of multi-steps reactions without parallel reaction steps. DAEM is reported to be an effective and accurate approach to simulate the pyrolysis of complex processes with several parallel first order and independent irreversible reactions (Wang et al., 2017). Also, DAEM is more theoretically stable and it is appropriate for the comparison of reactivities of different biomass species (Gupta et al., 2020). Hence, it has become the most widely used model in the investigation of biomass pyrolysis (Fang et al., 2020).

The experimental results for TG were analysed based on the kinetic parameters of thermal decomposition using iso-conversion models previously mentioned (Huang et al., 2018; Zou et al., 2019). The reaction rate is a function of change in conversion per unit time which is a function of the conversion degree (α), Eq. (3):

$$\frac{d\alpha}{dt} = k_0(T)f(\alpha) \tag{3}$$

The $f(\alpha)$ is the model of reaction for heterogeneous conversion process and reaction constant $k_0(T)$ is fundamentally governed by Arrhenius equation, which is an indication of the effect of temperature on the rate of reaction. Therefore, conversion degree α and $k_0(T)$ can be expressed as Eq.(4) and Eq.(5):

$$\alpha = \frac{m_0 - m_t}{m_0 - m_\infty} \tag{4}$$

where m_0 is the initial mass, m_t is the mass at the time t and m_∞ is the final mass of the residue as recorded using weigh balance.

$$k_0(T) = k_0 e^{-\frac{E_a}{RT}} \tag{5}$$

where k_0 is the compensation (pre-exponential) factor, E_a is the activation energy, T is the absolute temperature (K). Assuming that temperature is a function of time and increases with a constant heating rate $\beta(Ks^{-1})$, then β is given as Eq. (6)

$$\beta = \frac{dT}{dt} = \frac{dT}{d\alpha} \times \frac{d\alpha}{dt} \tag{6}$$

Therefore;

$$\frac{d\alpha}{dT} = \frac{k_0}{\beta} e^{-\frac{E_a}{RT}}.f(\alpha) \tag{7}$$

The combination of Eqs. (6) and (7) can be expressed as Eq. (8):

$$g(\alpha) = \int_0^\alpha \frac{k_0}{\beta} e^{-\frac{E_a}{RT}}\, dT = \frac{k_0 E_a}{\beta R} \int_y^\infty v^{-2} e^{-v} dv = \frac{k_0 E_a}{\beta R} P(y) \tag{8}$$

where $g(\alpha)$ signifies the integral form of the reaction model and $P(y)$ is an approximated temperature integral equation, with $y = \frac{E_a}{RT}$. It is noted that Eq. (8) is non-exact, as such does not have an exact solution, therefore an approximated solution for this integral expression is used on the development of iso-conversion methods. Rearrangement and approximation of Eq. (8) with $P(y) = y^{-2}e^{-y}$ is an expression of KAS method (Akahira, 1971; Kissinger, 1957) as in Eq. (9) while FWO method Eq. (10) is derived based on Doyle's approximation (Doyle, 1961). The approximation equation of Doyle and Murray-white are respectively associated with FWO and KAS methods (Alves et al., 2019).

$$\text{KAS: } ln\left(\frac{\beta}{T_p^2}\right) = ln\left(\frac{k_0 E_a}{Rg(\alpha)}\right) - \left(\frac{E_a}{RT}\right) \tag{9}$$

FWO: $ln\beta = ln\left(\frac{k_0 E_a}{Rg(\alpha)}\right) - 1.052\left(\frac{E_a}{RT}\right) - 5.331$ (10)

DAEM: $ln\left(\frac{\beta}{T^2}\right) = ln\left(\frac{k_0 R}{E_a}\right) - \left(\frac{E_a}{RT}\right) + 0.6575$ (11)

The slopes of Eqs. (9-11) are used to determine the E_a while the k_0 is determined from the intercept for $\alpha = 0 - 0.9$.

Table 1 presents the measuring instrument and the standard deviation for each measured variables. Based on the number of variables which were investigated, the total number of samples is seventy-two (72) with thirty- six (36) each for NT15 and NT25.

Table 1. Tropical almond properties and measuring instrument with standard deviation

Parameter	Units	Measuring equipment	Standard deviation	Number of replications
Volatile matter	%	Thermolyne Furnace 6000	0.02	3
Fixed carbon	%		0.02	3
Ash	%		0.02	3
Carbon, C	%	Thermo scientific FLASH 2000 CHNS analyser	0.12	3
Hydrogen, H	%		0.03	3
Nitrogen, N	%		0.009	3
Sulphur, S	%		0.002	3
Higher heating value	MJ/kg	Cal2k Eco calorimeter	0.02	3
TG analysis	%	STA 7200V TG Analyser		3
Pore size	nm	Micromeritics ASAP2460	0.001	3
Pore volume	cm^3/g			
Pore surface area	m^2/g			
FTIR (Transmittance peak)	%T	IRAffinity-1S	0.02	3
XRD	arb	Rigaku miniflex	0.02	3
Total number of sample				36

3. Results and Discussion

The energetic properties of the tropical almond were obtained and compared based on the particle sizes and this was further compared with other almond parts.

3.1. Proximate and Ultimate Analyses

The proximate and ultimate constituents of tropical almond blend for different particle sizes (NT25 and NT15) are presented in Table 2. The analysis of variance (ANOVA) for ultimate constituents at 95 % confidence level showed that there is no significant difference between the mean values of the ultimate constituents ($p = 0.6219, F = 0.6090 < F_{crit} = 3.4903$). Therefore, it can be concluded that ultimate properties may not be prominently affected by the particle size. It is noted that there is slightly higher VM and ash content in NT15 compared with NT25. This may be attributed to more rapid heating resulting from larger surface area, likely brittleness of inorganic materials and a reduced pore diffusion path length which could have led to the reduction in the extent of secondary interaction among the particles (Bridgeman et al., 2007; Liu and Bi, 2011).

Table 2. Ultimate (dry basis) and Proximate analysis (wet basis) of tropical almond blend

Sample	This study (NT15)	This study (NT25)
M %	6.70 ± 0.3	6.64±0.2
FC %	11.26±0.3	12.1±0.3
VM %	80.93±0.1	80.39±0.1
Ash %	1.11±0.07	0.87±0.09
C %	49.13±0.2	49.13±0.2
H %	5.23±0.1	5.23±0.1
O %	44.66±0.1	44.66±0.1
S %	0.02±0.001	0.02±0.001
N %	0.96±0.01	0.96±0.01
Cl %	0.02±0.002	0.02±0.002
HHV MJ/kg	25.07±0.2	23.26±0.3

Table 3 compares the present studies to the previous work on the almond which cut across the almond wood, hull, and shell. The proximate analysis was done on a wet basis while the elemental composition was determined on a dry basis. The FC is lowest in the tropical almond blend while it is highest in the almond hulls residue as presented in Table 3. Also, the ash content in almond shell residue is lowest compared to other almond parts and blended tropical almond residue. The higher ash content may be beneficial as the ash can be used as a catalyst in thermal conversion technologies (Brinchi et al., 2013). The molar ratio H:C and O:C is related to energy availability. The lowest H:C value which is approximately 1.26 was observed in tropical almond blend while the highest value (1.46) was found in almond shell. This is due to the presence of more energy in C-H bonds relative to C-C bonds of the tropical almond blend (Gómez et al., 2016; Jenkins et al., 1998).

Of interest is the S, Cl and N content of the tropical almond blend, since the essence is not only to determine the fuel properties of the biomass but also its potential contribution to greenhouse gas (GHG) emission (Olatunji et al., 2018). Almond hulls residue had the highest N content (1.2 %), while the tropical almond blend has the lowest S content (0.02 %). The lower S content in tropical almond blend is appealing for energy production since the formation of acidic rain is less likely (González et al., 2005). Cl plays a major role in deposit formation and its presence increases the corrosion of tubes used in biomass power plants. The average value of Cl (0.02 %) is the same with almond hulls and lesser than almond shells (0.06 %). However, varying properties may not be due to the blending and particle sizes only, but a combination of interacting factors such as growing condition, climate, soil and so on (Olatunji et al., 2018; Vassilev et al., 2010). The HHV of 25.07 MJ/kg and 23.26 MJ/kg were obtained for NT15 and NT25 respectively, which is higher than the values obtained for other samples (wood almond residue, almond hull, and shell).

Table 3. Comparative study of different almond biomass feedstock

Almond sample	This study (NT15)	This study (NT25)	Wood-almond residue (Miles et al., 1995)	Almond hulls (Jenkins et al., 1998)	Almond shell (Demirbas, 2004; González et al., 2005)
[a] M %	6.7	6.64	22.7	6.5	3.3
[a] FC	11.26	12.1	12.3	18.8	15.8
[a] VM %	80.93	80.39	59.7	69	80.3
[a] Ash %	1.11	0.87	5.3	5.7	0.6
[b] C %	49.13	49.13	52.4	59.6	50.3
[b] H %	5.23	5.23	6	6.4	6.2
[b] O %	44.66	44.66	41.2	41.7	42.5
[b] S %	0.02	0.02	0.04	0.07	0.05
[b] N %	0.96	0.96	0.4	1.2	1
[b] Cl %	0.02	0.02	0.03	0.02	0.06
H:C	1.26	1.26	1.36	1.28	1.46
O:C	0.68	0.68	0.59	0.52	0.63

HHV MJ/kg	25.07	23.26	18.35	18.89	18.2

[a] dry basis, [b] wet basis

The ash yield may not provide sufficient information when the composition is not known. Therefore, Table 4 presents the elemental oxides present in the ash of tropical almond blend. Ash composition varies with the biomass source. The degree of fouling, slagging and corrosion is closely related to ashes and elemental oxides which are released during thermal conversion (Vassilev et al., 2017). For all the samples, K_2O, SiO_2, and CaO respectively were the most abundant oxides: Tropical almond blend has 56 % K_2O, 16.65 % SiO_2 and 10.76 % CaO. Considering the ratio between SiO_2, CaO, and K_2O, the almond shell has the least tendency towards slagging, though higher value of chlorine (0.06 %) compared with other samples may lead to the formation of fouling compound when its Cl component react with K.

Table 4. Elemental oxides in ash from almond

Ash	SiO_2	CaO	K_2O	MgO	P_2O_5	Al_2O_3	SO_3	Fe_2O_3	Na_2O	TiO_2
Almond shell (Vassilev et al., 2010)	17.03	12.65	51.73	4.73	4.66	3.22	0.87	2.70	2.30	0.11
Almond hulls (Vassilev et al., 2010)	11.21	9.75	63.90	4.00	6.17	2.52	0.41	0.92	1.06	0.06
NT15	16.65	10.76	56.00	4.02	5.57	2.70	0.61	1.90	1.70	0.09
NT25	16.51	10.69	55.60	4.22	6.00	2.51	0.58	1.70	2.10	0.09

Also, the HHV was estimated as presented in Table 5 and 6 based on the empirical correlations derived from the proximate and ultimate analysis respectively. The correlation developed by Nhuchhen and Abdul Salam (2012) was the closest to the experimental values, while the estimation based on elemental composition showed the greatest deviation with the closest to the experimental value been Lloyd and Davenport (1980).

Table 5. Prediction based on proximate analysis

Correlation	Predicted value (MJ/kg) (NT15)	Predicted value (MJ/kg) (NT25)	Min dev	Ref
$\mathbf{HHV = 19.2880 - 0.2135(\frac{VM}{FC}) - 1.9584(\frac{Ash}{VM}) + 0.0234(\frac{FC}{Ash})}$	20.90	21.01	4.17	(Nhuchhen and Abdul Salam, 2012)
$\mathbf{HHV = 0.3536FC + 0.1559VM - 0.0078Ash}$	16.46	16.80	8.61	(Parikh et al., 2005)
$\mathbf{HHV = 0.3543FC + 0.1708VM}$	17.68	18.02	7.39	(Cordero et al., 2001)
$\mathbf{HHV = 0.2521FC + 0.1905VM}$	18.10	18.36	6.97	(Yin, 2011)

Table 6. Prediction based on ultimate analysis

Model	Predicted value (MJ/kg)	Max dev	Ref
$\mathbf{HHV = 0.230C + 0.761H + 1.247N + 14.259}$	30.74	5.67	(Abbas et al., 2013)
$\mathbf{HHV = 0.3708C + 0.0011124H - 0.1391O + 0.3178N + 0.1391S}$	12.32	12.75	(Meraz et al., 2003)
$\mathbf{HHV = 0.3578C + 1.1357H - 0.0845O + 0.059N + 0.1119S}$	19.80	5.27	(Lloyd and Davenport, 1980)
$\mathbf{HHV = 0.3515C + 1.1617H - 0.1109O + 0.06276N + 0.1046S}$	18.45	6.62	(Boie, 1953)

3.2. BET analysis

The surface properties of the tropical almond blend are given in Table 7. Apparently, pore surface area of 0.970-1.218m²/g are in agreement with literature values (Barakat et al., 2014; Leal et al., 2019; Zu et al., 2014) and the pore volume and pore size are within the same range. An inverse relationship was observed between the particle size and the surface areas. The higher surface area obtained for lower particle size may affect the reactivity such

that NT15 is more reactive with better dispersion of active site and heat transfer rate than NT25 (Ndolomingo et al., 2020).

Table 7. Surface properties of tropical almond blend from N_2 adsorption

Particle size (μm)	Volume (cm^3/g)	Surface area (m^2/g)	Pore size (nm)
NT15	0.008209	1.218	27
NT25	0.007473	0.970	31
SD	±0.0001	±0.04	±0.3

Adsorption/desorption isotherms provide vital information about the pore structure which helps to quantitatively determine the pore type. Fig. 3 and 4 show the isotherm plot and pore size distribution for tropical almond, based on different particle sizes (NT15 and NT25). Similar patterns were noticed for both NT15 and NT25. The adsorption isotherm does not display any significant broad hysteresis loop since there is close matching between the adsorption and desorption process. The close matching between the desorption and adsorption curve may be an indication of the thermal stability of the sample. There are two characteristic regions noticed in the adsorption branch which are; lower pressure ($P/P_o<0.9$) where the adsorption rate was lower and higher relative pressure ($0.9 < P/P_o < 1$) where the uptake of a major amount of nitrogen took place (Ji et al., 2016; Mena-Durán et al., 2019). The adsorption-desorption curves are majorly horizontal over a wide interval of pressures but a slight difference in quantity absorbed between the particle sizes was noted at the pressure range $0.7 < P/P_o < 0.95$.

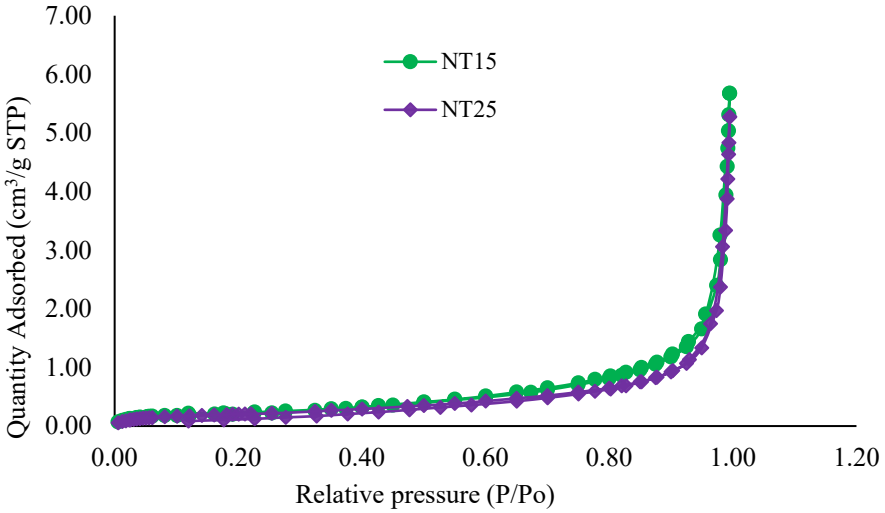

Fig. 3. N_2 sorption isothermal plot for the tropical almond blend

The pore size distribution curve in Fig. 4 with an exploded view, reveals the full range of data as obtained from the experiment. Based on IUPAC, pore with a diameter less than 2nm are classified as micropores; pores with a diameter greater than 50nm are defined as macropores; while the pores with a diameter of 2-50nm are defined as mesopores. The curves indicate the presence of micropores of various sizes with the highest distribution of micropores which are less than 2nm. This further shows that micropores have the most significant contribution to the surface area and average pore diameter. Although, both NT15 and NT25 have large proportions of micropores, the variation in the pore size distribution for the particle sizes is expected since the particles were ground to different sizes over different period.

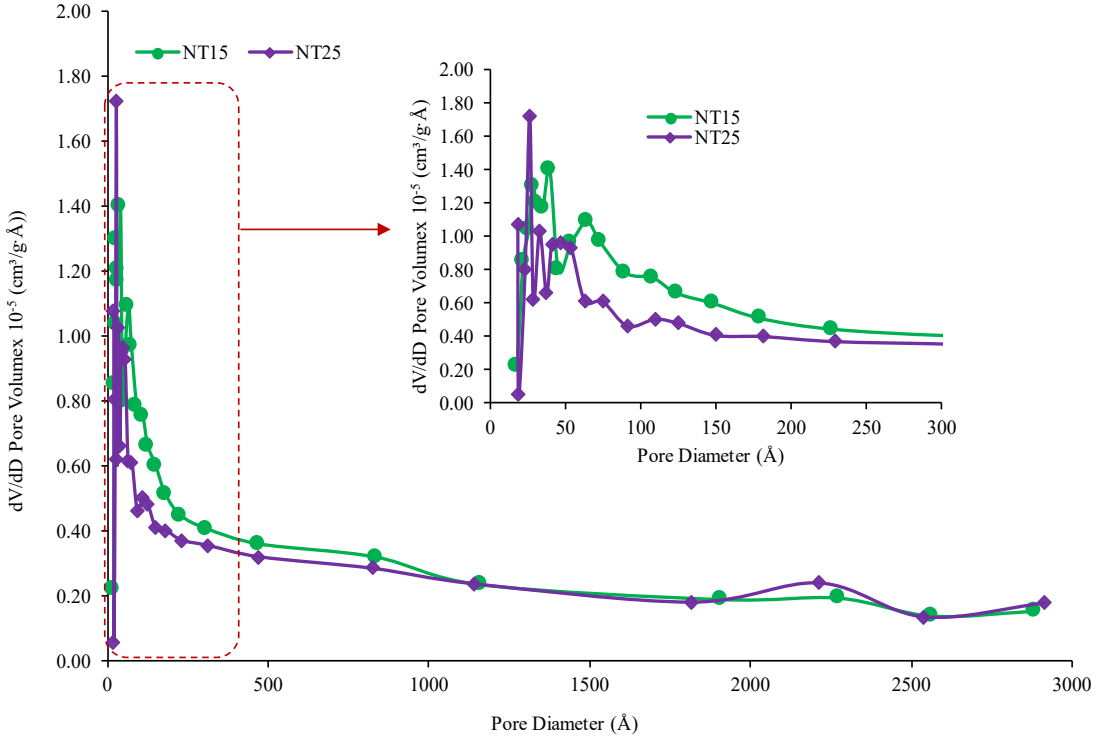

Fig. 4. Pore size distribution for tropical almond blend

3.3. Scanning Electron Microscopy (SEM)

SEM images of tropical almond particles are given in Fig. 5 and 6. The surface of Fig. 5 appears smoother, with more closely packed grains and more visible microfibril. The microfibril with heterogeneous distribution of micropores and rough texture noted in the NT15 may be an indication of varying resistance to degradation (Ämmälä et al., 2019).

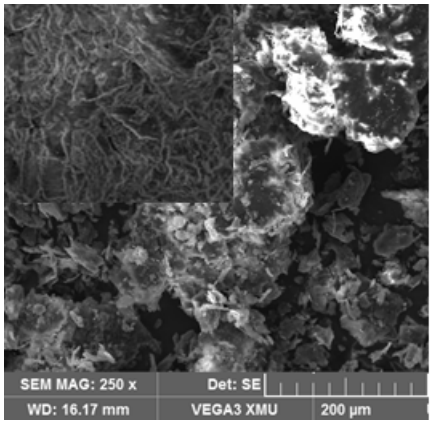

Fig. 5. SEM image NT15

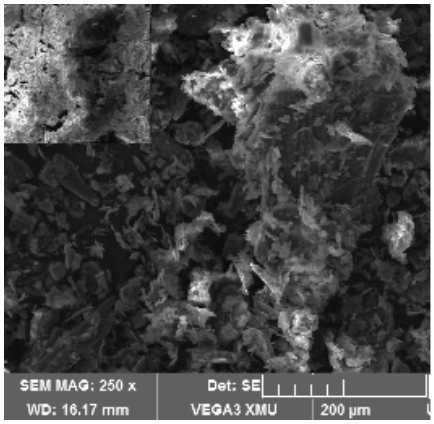

Fig. 6. SEM image NT25

3.4. X-ray Diffraction Analysis (XRD)

Table 8 presents the XRD analysis with the information about the crystallinity indices as a function of absorption peak for the tropical almond blends of different particle sizes. The crystallinity of the surface of biomass is mainly due to the high molecular hydrocarbon and fatty components (Chen et al., 2019), though the overall crystallinity is a broad function of the complex nature of bonding between the cellulose, hemicellulose, and lignin. The peak intensity, I_{002} and I_{arm} were obtained at 2θ=22.06^0 and 17.64^0 respectively for NT15 while it was obtained at 2θ=21.04^0 and 16.06^0 respectively for NT25. The analysis revealed diverse crystalline structure in this biomass. The Cr_I was lesser (36.72%) in NT25 compared to NT15 (39.43%). This may be due to a prolonged period of mechanical actions such as shearing, and impact (Karimi and Taherzadeh, 2016). Also, greater Cr_I means that cellulose in the biomass feedstock has a higher percentage of the crystalline region compared to the amorphous region. It may be suggested that NT15 will be more biodegradable based on several investigations which have

shown that biodegradability increases with higher crystallinity (Karimi and Taherzadeh, 2016). Easily biodegradable materials are of advantage in energy generation from biomass, especially in the pyrolytic conversion process.

Table 8. Crystallinity Indices of tropical almond

Almond **blend**	I_{002}	I_{arm}	**Crystallinity index** (Cr_I)	**Crystallite size** (D_{002})
NT15	1002	822	39.43	3.54
NT25	1180	852	36.72	3.46

Also, high angle, HA diffraction curve is shown in Fig. 7. The broad peak in NT25 which reflects the crystalline system in the sample is lesser than NT15. The sudden change in peak may be due to different (cellulosic) components of tropical almond which were blended. The steepness of these peaks is an indication of the changes which may take place during thermochemical processing of biomass (Xu et al., 2013).

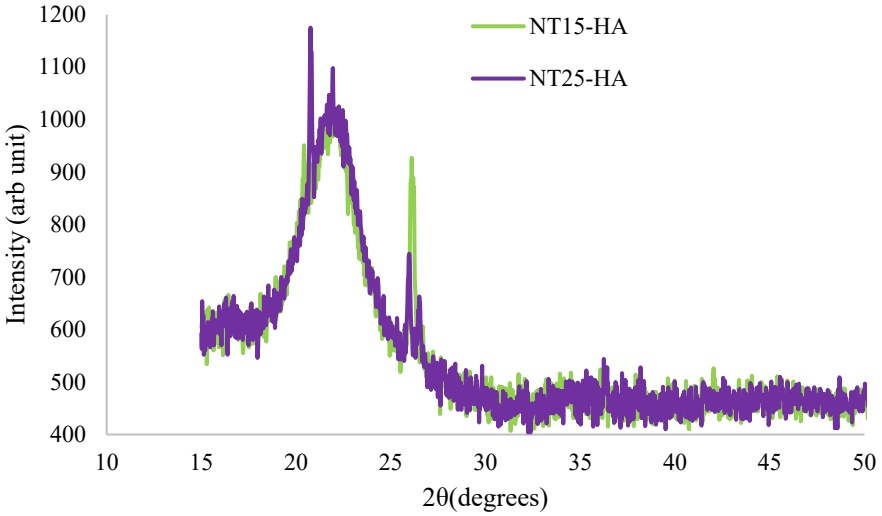

Fig. 7. Tropical Almond high angle diffraction

3.5. Fourier Transform Infrared analysis

The FTIR analysis in Fig. 8 shows the functional groups which are present in tropical almond blend. It reflects a range of peaks which represent mixed functional groups that are available in this sample.

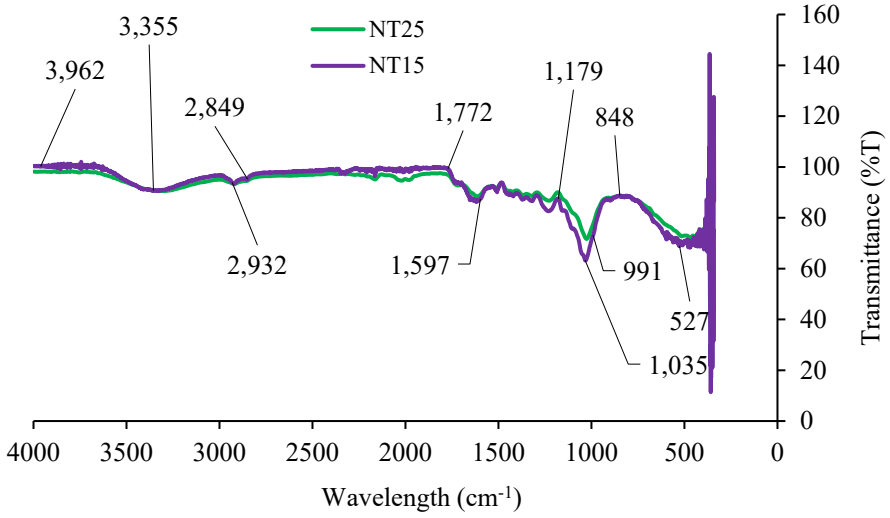

Fig. 8. FTIR of tropical almond blends showing different peaks

From Table 9, the most prominent spectra peak occurs at 1035 cm^{-1} and it indicates the presence of C-O, C=C, and C-C-O stretching. The peaks in the range of 3450-2860 cm^{-1} reveal the presence of spectrum originating from -OH stretching, aliphatic C-H stretching bonds and stretching mode of carbonyl, mainly aldehyde, ketones, and ester. It is noted that there were no significant differences among the functional groups present in the two particle sizes. This means that the composition of structural elements is proximately the same for the two particle sizes. All the peaks observed in the two feedstocks fall within the same band positions, meaning that the same functional group can be found in both NT15 and NT25. However, the spectra peaks were different along some band positions for the two particle sizes.

Table 9. FTIR functional groups

Band position (cm^{-1})	Assigned band
480, 554	Aromatic ring, C-C stretching
782, 815	C-H alkynes bending, C-H phenyl ring substitution bands
875	Glycosidic linkage
990	C-O valency vibration
1035	C-O, C=C and C-C-O stretching
1175	Alcohol C-O stretches, ethers, carboxylic acids
1200,1215	O-H stretching, C-C + C-O stretch
1270,1280	Aromatic ring vibration, Aromatic C-O stretching
1,516,1616	Aromatic C-C ring stretching, C-H phenyl ring substitution overtones
2860,2928	Aldehydes C-O stretches, esters, ketones, carboxylic acids, Alkanes/aliphatic C-H stretching
3200-3650	-OH stretching

Sources: (Schwanninger et al., 2004; Singh et al., 2017)

3.6. TG analysis

3.6.1. Effect of heating rate on thermal properties

The pyrolysis of the tropical almond at the temperature range of 25-980 ^{0}C is shown in Fig. 9. The mass reduction in the temperature from 60-200 ^{0}C was due to an initial moisture release. A single point of inflexion was observed on the TG curve. The increase in the heating rate appears to shift the curve to higher temperatures, possibly due thermal hysteresis effect which is related to the resistance of the material (Naik et al., 2010; Niu et al., 2013). The maximum weight loss (around 60 %) occur between 250 ^{0}C and 350 ^{0}C. This significant weight loss is due to dissociation and decomposition of the chemical bonds. Also, volatile hydrocarbon, cellulose, and hemicellulose and some part of lignin are given off. Above 400 ^{0}C, there is a rapid change in the TG slope, which informed the slower weight loss as the temperature further increases. The remaining chars degrade at 500 ^{0}C and above, though at a different rate depending on the heating rate of the sample. The degradation becomes relatively stable at 800 ^{0}C. From the Derivative thermogravimetry, DTG distribution curve, as the temperature increases, the weight loss increases, until it reaches a peak after which the weight loss rapidly decreased despite the increase in temperature. The magnitude of this peak is possibly due to the inherent moisture content of the sample (Yu et al., 2005). The sharp peak between 325 ^{0}C and 350 ^{0}C is due to the loss of cellulose and hemicellulose. As the heating rate increases from 10-30 ^{0}C min^{-1}, the weight loss of the tropical almond increases and the peak value of the DTG curve shifted to a higher temperature.

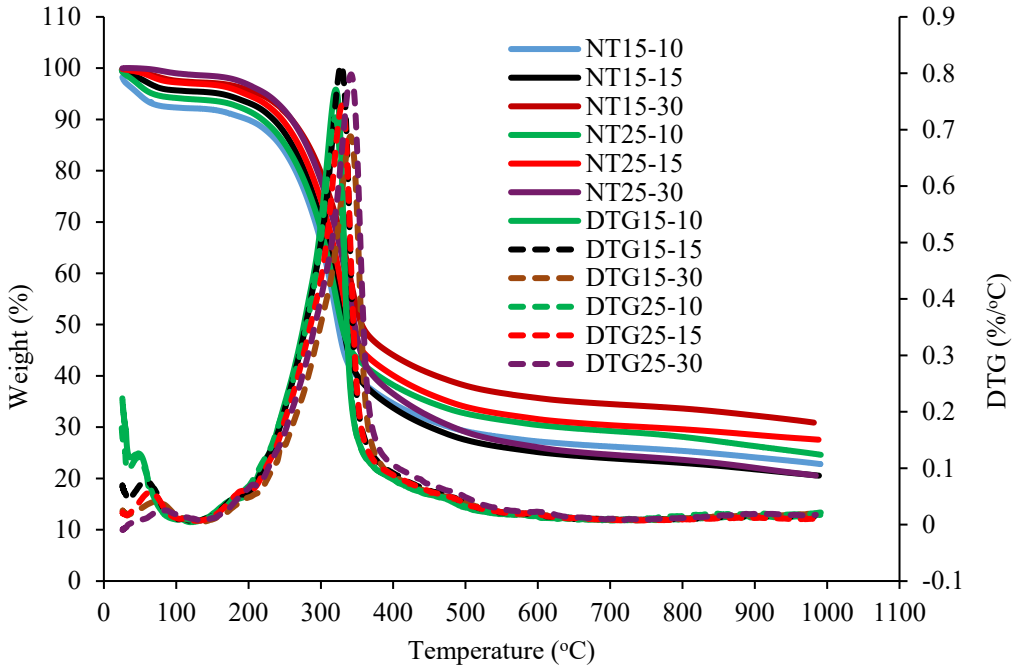

Fig. 9. TG and DTG of tropical almond blends.

3.6.2. Effect of particle size on the pyrolysis

The TG/DTG curves obtained at the heating rate of 15 ^{0}C/mins for different particle sizes are presented in Fig. 10. The two different particles (NT15 and NT25) have a similar point of inflexion though with larger particle size (NT25), the curve slightly shifted toward higher temperatures, due to increase in heating time (Bidabadi et al., 2015; Mlonka-Mędrala et al., 2019). Consequentially, a limitation is placed on the volatiles evolving during pyrolysis which may lead to a decrease in the yield of pyrolysis gas (Lu et al., 2010). However, it is observed that the DTG curve for both particle sizes follows the same profile though at different peak values. The peak temperature of the NT25 and NT15 are 332 ^{0}C and 329 ^{0}C respectively.

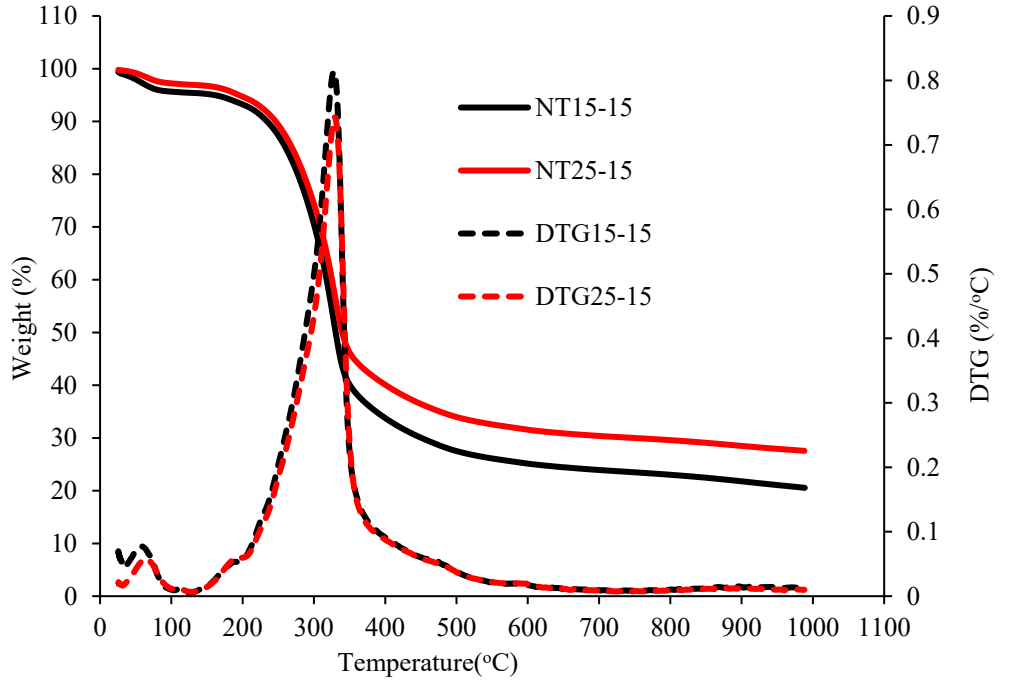

Fig. 10. Effect of particle sizes on the thermal behaviour

3.7.3 Determination of Kinetic Parameters

It has been reported that the apparent activation energy is a function of fractional conversion since most pyrolysis follows multi-step reaction, therefore varying degrees of conversion from 0.2-0.9 were used to determine the kinetic parameters in this study. To evaluate the kinetic variables of blended tropical almond, the same conversion rates were selected for the three models at different heating rates, i.e., from 10, 15, and 30 $^{o}Cmin^{-1}$.

The effect of particle sizes on the kinetic parameters of blended tropical almond was reported in Table 10. The activation energy and the compensation effects were calculated for α, the values indicated that E_a is highly dependent on α resulting from the multistep reactions due to the release of volatiles in the course of pyrolysis (Wang et al., 2019; Zou et al., 2019). The R^2 values for all α were greater than 0.99 except α=0.2. Also, E_a and k_0 progressively varies with α, which further confirm that there is multi-reaction mechanism in blended tropical almond pyrolysis. At α=0.2, the lower energy (E_a) required to initiate the reaction may be due to weak intermolecular bonding among the particles (Mehmood et al., 2017; Zou et al., 2019). E_a estimated by FWO was higher than other methods for all α. The E_a estimate for both KAS and DAEM were the same though with different pre-exponential factors. The ANOVA between the average E_a of each particle size at 95 % confidence level showed that there is a statistically significant difference in kinetic parameters ($p = 0.00036, F = 27447.5 > F_{crit} = 18.5$). The average E_a for NT15 and NT25 were in the range of 127.1-131 $kJmol^{-1}$ and 129-133 $kJmol^{-1}$ respectively for all the three methods, with the lowest E_a (127.4 $kJmol^{-1}$) obtained for the smaller particle size (NT15). Vo et al. (2017) suggested that the lower value E_a indicates lower costs of pyrolysis, therefore, NT15 may have better applicability considering the costs of pyrolysis.

Table 10. E_a, A and R^2 value of NT15 and NT25 based on KAS, DAEM and FWO

Size	α	KAS			DAEM			FWO		
		$E_a(kJmol^{-1})$	A (min^{-1})	R^2	$E_a(kJmol^{-1})$	A (min^{-1})	R^2	$E_a(kJmol^{-1})$	A (min^{-1})	R^2
	0.2	72.4	4.74E+06	0.7207	72.4	2.45E+06	0.7207	77.3	2.59E+07	0.7648
	0.3	117.0	5.52E+10	0.9914	117.0	2.86E+10	0.9914	120.1	1.31E+11	0.9925
	0.4	130.8	4.79E+11	0.9964	130.8	2.48E+11	0.9964	133.5	9.75E+11	0.9969
	0.5	136.9	9.21E+11	0.9965	136.9	4.77E+11	0.9965	139.5	1.79E+12	0.9969
NT15	0.6	148.9	6.50E+12	0.9994	148.9	3.37E+12	0.9994	151.0	1.11E+13	0.9995
	0.7	146.4	2.31E+12	1.0000	146.4	1.20E+12	1.0000	148.9	4.22E+12	1.0000
	0.8	131.8	2.78E+10	0.9965	131.8	1.44E+10	0.9965	135.5	6.90E+10	0.9970
	0.9	132.6	8.82E+08	0.9970	132.6	4.57E+08	0.9970	137.9	2.87E+09	0.9975
	Avg	**127.1**	**1.29E+12**		**127.1**	**6.66E+11**		**130.5**	**2.29E+12**	
	0.2	75.7	1.05E+07	0.9404	75.7	5.44E+06	0.9404	80.5	5.31E+07	0.9515
	0.3	107.2	5.61E+09	0.9773	107.2	2.91E+09	0.9773	110.8	1.59E+10	0.9806
	0.4	119.8	4.02E+10	0.9851	119.8	2.08E+10	0.9851	123.1	9.75E+10	0.9871
	0.5	131.3	2.58E+11	0.9916	131.3	1.34E+11	0.9916	134.2	5.47E+11	0.9927
NT25	0.6	142.7	1.68E+12	0.9965	142.7	8.73E+11	0.9965	145.2	3.14E+12	0.9969
	0.7	147.9	2.68E+12	1.0000	147.9	1.39E+12	1.0000	150.3	4.86E+12	1.0000
	0.8	164.3	9.00E+12	0.9139	164.3	4.67E+12	0.9139	166.6	1.51E+13	0.9236
	0.9	147.1	6.54E+09	0.7570	147.1	1.98E+02	0.7570	151.7	8.09E+03	0.8840
	Avg	**129.5**	**1.71E+12**		**129.5**	**8.86E+11**		**132.8**	**2.97E+12**	

4. Energy benefits and emission reduction potential

The energy benefits and emission reduction potential for the replacement of fossil fuel such as oil, coal and natural gas with biofuels are determined based on Eq. 12 with fossil fuel as the baseline since the HHV and the almond production for each country is known (FAO, 2019).

$$E_p = P_{NT} \cdot f_s \cdot RH \cdot HHV \cdot U_c \quad (12)$$

E_p is the potential energy production from the whole tropical almond (MWh), P_{NT} is the almond production in a given country (kg) based on 2019 data, f_s is a factor of residue in an almond fruit, and U_c is a unit conversion (0.000277778 WhJ^{-1}). Tropical almond blend is made from the blending of almond hulls and shells. Based on the recent data, almond residue (hull and shell) represent 73 % of the total almond weight (ABOC, 2018), therefore f_s is assumed at 73 %. Table 11 gives the almond produced in some major countries in the world with the equivalent energy potential and CO_2 reduction for the year 2017 (Outlook, 2018). Since CO_2 is the major component of GHG, a reasonable approximation of total GHG emission can be obtained by converting all other GHG to CO_2 equivalent (Ma, 1998; Perea-Moreno et al., 2018). The highest energy potential was obtained in the USA, Spain, and Morocco in that order. The comparison of total emission across different countries showed that Morocco has the highest emission reduction. For a country such as Morocco which heavily depends on imported fossil fuel to meet its energy demand, and with ambition to increase the renewable energy uptake to 52 % of the electric balance sheet by 2030 (Saghir and Naimi, 2019; Schinke et al., 2016), application of almond residue in biofuel production would be an interesting option both in term of energy potential and CO_2 emission reduction (3.28 %).

Table 11. Energy and CO_2 emission reduction potential of almond blend in 2017

Country	CO_2 2017 (Mtonnes)	P_c(tons)	E_p (GWh)	Mtoe	Mtonnes	% CO_2 reduction
USA	5014.14	1,029,655	48,523.10	4.17	17.32	0.35
Spain	299.90	255,503	12,040.73	1.04	4.30	1.43
Morocco	60.00	116,923	5,510.07	0.47	1.97	3.28
Iran	622.10	111,845	5,270.76	0.45	1.88	0.30
Turkey	388.50	90,000	4,241.30	0.36	1.51	0.39
Italy	346.30	79,599	3,751.15	0.32	1.34	0.39
Australia	412.30	75,373	3,552.00	0.31	1.27	0.31
Algeria	127.80	61,943	2,919.10	0.25	1.04	0.82
China	9229.80	51,953	2,448.32	0.21	0.87	0.01
World	**33242.50**	**2,239,697**	**105,547.05**	**9.08**	**37.68**	**0.11**

5. Conclusion

The physico-chemical, energy benefits, thermal analysis and emission reduction potential of blended almond were evaluated. The effect of particle sizes on the proximate, ultimate, and thermal behaviour of this feedstock was reported. The results obtained proved that particle size reduction can enhance the reactivity of fuel and should be considered at the planning stage of thermal conversion process. The estimated values of E_a at various conversion orders showed the existence of multi-step reaction scheme. The HHV of tropical almond (25.07 MJ/kg) is greater than other almond feedstocks reviewed from the previous studies. In term of emission reduction potential, a country like Morocco would have significant CO_2 emission savings. While the materials from blended almond residue may not provide the entire feedstock needed for sustainable biofuel production, its application will be beneficial in modular energy production. The information obtained from the kinetic parameters may be useful in the control, simulation, and optimization of thermochemical process. Comprehensive knowledge of the characteristics of biomass can assist in industrial thermochemical process development with overall benefits of clean, cost-efficient and eco-friendly bioenergy production.

Data availability statement

The raw data required to produce these findings cannot be shared at this time as data also forms a part of an ongoing study. However, it can be made available on request.

References

Abbas, A., Ibrahim, A., Muttalib, M., Aris, M., 2013. Fuel Characterization and Energy Prediction of Malaysian Poultry Processing. Asian Journal of Scientific Research 6(3), 498-507.

ABOC, A.B.o.C., 2018. Almond tree fruit weight-2017/2018 crop year https://www.almonds.com/sites/default/files/17-18_whole_crop_position_report_addendum.pdf accessed on 19/09/2019.

Agency, I.E., 2018. Bioenergy and biofuels. https://www.iea.org/topics/renewables/bioenergy/ accessed on 27th Novemeber, 2018.

Akahira, T., 1971. Trans. Joint convention of four electrical institutes. Res. Rep. Chiba Inst. Technol. 16, 22-31.

Akubude, V.C., Nwaigwe, K.N., 2016. Economic Importance of Edible and Non-edible Almond Fruit as Bioenergy Material: A Review. American Journal of Energy Science 3(5), 31-39.

Álvarez, A., Pizarro, C., García, R., Bueno, J., Lavín, A., 2016. Determination of kinetic parameters for biomass combustion. Bioresource technology 216, 36-43.

Alves, J.L.F., da Silva, J.C.G., da Silva Filho, V.F., Alves, R.F., de Araujo Galdino, W.V., De Sena, R.F., 2019. Kinetics and thermodynamics parameters evaluation of pyrolysis of invasive aquatic macrophytes to determine their bioenergy potentials. Biomass and bioenergy 121, 28-40.

Ämmälä, A., Laitinen, O., Sirviö, J.A., Liimatainen, H., 2019. Key role of mild sulfonation of pine sawdust in the production of lignin containing microfibrillated cellulose by ultrafine wet grinding. Industrial Crops and Products 140, 111664.

Bajpai, P., 2019. Fuel Potential of Third Generation Biofuels, Third Generation Biofuels. Springer, pp. 7-10.

Barakat, A., Mayer-Laigle, C., Solhy, A., Arancon, R.A., De Vries, H., Luque, R., 2014. Mechanical pretreatments of lignocellulosic biomass: towards facile and environmentally sound technologies for biofuels production. Rsc Advances 4(89), 48109-48127.

Bidabadi, M., Moghaddam, M.R., Mostafavi, S.A., Dizaji, F.F., Dizaji, H.B., 2015. An analytical model for pyrolysis of a single biomass particle. Journal of Central South University 22(1), 350-359.

Bingwa, N., Patala, R., Noh, J.-H., Ndolomingo, M.J., Tetyana, S., Bewana, S., Meijboom, R., 2017. Synergistic effects of gold–palladium nanoalloys and reducible supports on the catalytic reduction of 4-nitrophenol. Langmuir 33(28), 7086-7095.

Boie, W., 1953. Fuel technology calculations. Energietechnik 3, 309-316.

Bridgeman, T., Darvell, L., Jones, J., Williams, P., Fahmi, R., Bridgwater, A., Barraclough, T., Shield, I., Yates, N., Thain, S., 2007. Influence of particle size on the analytical and chemical properties of two energy crops. Fuel 86(1-2), 60-72.

Brinchi, L., Cotana, F., Fortunati, E., Kenny, J., 2013. Production of nanocrystalline cellulose from lignocellulosic biomass: technology and applications. Carbohydrate Polymers 94(1), 154-169.

Cai, J., He, Y., Yu, X., Banks, S.W., Yang, Y., Zhang, X., Yu, Y., Liu, R., Bridgwater, A.V., 2017. Review of physicochemical properties and analytical characterization of lignocellulosic biomass. Renewable and Sustainable Energy Reviews 76, 309-322.

Chen, X.-j., LIN, Q.-m., Rizwan, M., Zhao, X.-r., LI, G.-t., 2019. Steam explosion of crop straws improves the characteristics of biochar as a soil amendment.

Cordero, T., Marquez, F., Rodriguez-Mirasol, J., Rodriguez, J., 2001. Predicting heating values of lignocellulosics and carbonaceous materials from proximate analysis. Fuel 80(11), 1567-1571.

Crystal-Impact, M.v., 2013. http://www.crystalimpact.com/match/.

D3682-13, A., 2013. Standard Test Method for Major and Minor Elements in Combustion Residues from Coal Utilization Processes.

DDS, D.D.S.P.L., 2018. Eco Operating Manual. http://www.ddscalorimeters.com/ accessed on 28/11/2018.

de Oliveira Neto, G.C., Correia, J.M.F., Silva, P.C., de Oliveira Sanches, A.G., Lucato, W.C., 2019. Cleaner Production in the textile industry and its relationship to sustainable development goals. Journal of Cleaner Production 228, 1514-1525.

Demirbas, A., 2004. Combustion characteristics of different biomass fuels. Progress in energy and combustion science 30(2), 219-230.

Doyle, C.D., 1961. Kinetic analysis of thermogravimetric data. Journal of applied polymer science 5(15), 285-292.

E776-16, A., 2016. Standard Test Method for Determination of Forms of Chlorine in Refuse-Derived Fuel.

E871-82, A., 2013. Standard test method for moisture analysis of particulate wood fuels. West Conshohocken, PA: ASTM International.

E872-82, A., 2013. Standard test method for volatile matter in the analysis of particulate wood fuels. West Conshohocken, PA: ASTM International.

E1755-01, A., 2015. Standard test method for ash in biomass. West Conshohocken, PA: ASTM International.

E1757-01, A., 2015. Standard Practice for Preparation of Biomass for Compositional Analysis. PA: America society for Testing materilas, International.

Encyclopedic, 2019. https://www.nationalgeographic.org/encyclopedia/tropics/ accessed on 07/09/2019.

Esfahlan, A.J., Jamei, R., Esfahlan, R.J., 2010. The importance of almond (Prunus amygdalus L.) and its by-products. Food chemistry 120(2), 349-360.

Fang, S., Lin, Y., Lin, Y., Chen, S., Shen, X., Zhong, T., Ding, L., Ma, X., 2020. Influence of ultrasonic pretreatment on the co-pyrolysis characteristics and kinetic parameters of municipal solid waste and paper mill sludge. Energy 190, 116310.

FAO, F.a.A.O.o.t.U.N., 2019. FAOSTAT-CROPS. http://www.fao.org/faostat/en/#data/QC accessed on 09/04/2019.

Gómez, N., Rosas, J.G., Cara, J., Martínez, O., Alburquerque, J.A., Sánchez, M.E., 2016. Slow pyrolysis of relevant biomasses in the Mediterranean basin. Part 1. Effect of temperature on process performance on a pilot scale. Journal of cleaner production 120, 181-190.

González, J.F., González-García, C.M., Ramiro, A., Gañán, J., González, J., Sabio, E., Román, S., Turegano, J., 2005. Use of almond residues for domestic heating. Study of the combustion parameters in a mural boiler. Fuel processing technology 86(12-13), 1351-1368.

Gupta, A., Thengane, S.K., Mahajani, S., 2020. Kinetics of pyrolysis and gasification of cotton stalk in the central parts of India. Fuel 263, 116752.

Holzwarth, U., Gibson, N., 2011. The Scherrer equation versus the'Debye-Scherrer equation'. Nature nanotechnology 6(9), 534.

Huang, J., Liu, J., Chen, J., Xie, W., Kuo, J., Lu, X., Chang, K., Wen, S., Sun, G., Cai, H., 2018. Combustion behaviors of spent mushroom substrate using TG-MS and TG-FTIR: Thermal conversion, kinetic, thermodynamic and emission analyses. Bioresource technology 266, 389-397.

IEA, 2018. Modern bioenergy leads the growth of all renewables to 2023, according to latest IEA market forecast. https://www.iea.org/newsroom/news/2018/october/modern-bioenergy-leads-the-growth-of-all-renewables-to-2023-according-to-latest-.html (accessed on 12/11/2019).

Jenkins, B., Baxter, L., Miles Jr, T., Miles, T., 1998. Combustion properties of biomass. Fuel processing technology 54(1-3), 17-46.

Ji, T., Chen, L., Mu, L., Yuan, R., Knoblauch, M., Bao, F.S., Shi, Y., Wang, H., Zhu, J., 2016. Green processing of plant biomass into mesoporous carbon as catalyst support. Chemical Engineering Journal 295, 301-308.

Karimi, K., Taherzadeh, M.J., 2016. A critical review of analytical methods in pretreatment of lignocelluloses: composition, imaging, and crystallinity. Bioresource technology 200, 1008-1018.

Khiari, B., Jeguirim, M., Limousy, L., Bennici, S., 2019. Biomass derived chars for energy applications. Renewable and Sustainable Energy Reviews 108, 253-273.

Kissinger, H.E., 1957. Reaction kinetics in differential thermal analysis. Analytical chemistry 29(11), 1702-1706.

Leal, J.H., Moore, C.M., Sutton, A.D., Semelsberger, T.A., 2019. Surface energy of air fractionated corn stover. Industrial Crops and Products 137, 628-635.

Liu, X., Bi, X.T., 2011. Removal of inorganic constituents from pine barks and switchgrass. Fuel processing technology 92(7), 1273-1279.

Lizunkov, V., Politsinskaya, E., Malushko, E., Kindaev, A., Minin, M., 2018. Population of the world and regions as the principal energy consumer. International journal of energy economics and policy 8(3), 250-257.

Lloyd, W.G., Davenport, D.A., 1980. Applying thermodynamics to fossil fuels: Heats of combustion from elemental compositions. Journal of chemical education 57(1), 56.

Lu, H., Ip, E., Scott, J., Foster, P., Vickers, M., Baxter, L.L., 2010. Effects of particle shape and size on devolatilization of biomass particle. Fuel 89(5), 1156-1168.

Ma, Q., 1998. Greenhouse Gases: Refining the Role of Carbon Dioxide. NASA Goddard Institute for Space Studies. http://www. giss. nasa. gov/research/intro/ma 1.

Mehmood, M.A., Ye, G., Luo, H., Liu, C., Malik, S., Afzal, I., Xu, J., Ahmad, M.S., 2017. Pyrolysis and kinetic analyses of Camel grass (Cymbopogon schoenanthus) for bioenergy. Bioresource technology 228, 18-24.

Mena-Durán, C.J., Quintana, P., Barbosa, R., Baas, J., Escobar, B., 2019. Characteristics of Hydrochars Prepared from Cassava Residues Using Different Aqueous Media. Waste and Biomass Valorization, 1-6.

Meraz, L., Domínguez, A., Kornhauser, I., Rojas, F., 2003. A thermochemical concept-based equation to estimate waste combustion enthalpy from elemental composition☆. Fuel 82(12), 1499-1507.

Miles, T.R., Miles Jr, T., Baxter, L., Bryers, R., Jenkins, B., Oden, L., 1995. Alkali deposits found in biomass power plants: A preliminary investigation of their extent and nature. Volume 1. National Renewable Energy Lab., Golden, CO (United States); Miles (Thomas R ….

Mlonka-Mędrala, A., Magdziarz, A., Dziok, T., Sieradzka, M., Nowak, W., 2019. Laboratory studies on the influence of biomass particle size on pyrolysis and combustion using TG GC/MS. Fuel 252, 635-645.

Naik, S., Goud, V.V., Rout, P.K., Jacobson, K., Dalai, A.K., 2010. Characterization of Canadian biomass for alternative renewable biofuel. Renewable energy 35(8), 1624-1631.

Ndolomingo, M.J., Bingwa, N., Meijboom, R., 2020. Review of supported metal nanoparticles: synthesis methodologies, advantages and application as catalysts. Journal of Materials Science, 1-47.

Nhuchhen, D.R., Abdul Salam, P., 2012. Estimation of higher heating value of biomass from proximate analysis: A new approach. Fuel 99, 55-63.

Niu, Y., Tan, H., Liu, Y., Wang, X., Xu, T., 2013. The effect of particle size and heating rate on pyrolysis of waste capsicum stalks biomass. Energy Sources, Part A: Recovery, Utilization, and Environmental Effects 35(17), 1663-1669.

Nozela, W., Braz, C., Almeida, S., Ribeiro, C., Crespi, M., 2018. Mixture of biomass to energy reuse. Journal of Thermal Analysis and Calorimetry 131(1), 765-769.

Okoroigwe, E.C., 2015. Combustion Analysis and Devolatilazation Kinetics of Gmelina, Mango, Neem and Tropical Almond Woods under Oxidative Condition. International Journal of Renewable Energy Research (IJRER) 5(4), 1024-1033.

Olatunji, O., Madushele, N., Adedeji, P., Akinlabi, S., Ndolomingo, M., 2020. Geospatial investigation of physicochemical properties and thermodynamic parameters of biomass residue for energy generation. Biomass Conversion and Biorefinery, 1-15.

Olatunji, O.O., Ajayi, O., Mashinini, P., Nkosinathi, M., 2018. Experimental investigation of thermal properties of Lignocellulosic biomass: A review. IOP Conference Series: Materials Science and Engineering 413(1), 012054.

Olatunji, O.O., Akinlabi, S., Madushele, N., Adedeji, P.A., 2019. Estimation of the Elemental Composition of Biomass Using Hybrid Adaptive Neuro-Fuzzy Inference System. BioEnergy Research, 1-11.

Onsree, T., Tippayawong, N., Zheng, A., Li, H., 2018. Pyrolysis behavior and kinetics of corn residue pellets and eucalyptus wood chips in a macro thermogravimetric analyzer. Case Studies in Thermal Engineering 12, 546-556.

Outlook, B.E., 2018. Statistical Review of World Energy – all data, 1965-2017 - BP. https://www.bp.com/content/dam/bp/.../excel/energy.../bp-stats-review-2018-all-data.xls accessed on 12th January 2018.

Parikh, J., Channiwala, S., Ghosal, G., 2005. A correlation for calculating HHV from proximate analysis of solid fuels. Fuel 84(5), 487-494.

Perea-Moreno, A.-J., Perea-Moreno, M.-Á., Dorado, M.P., Manzano-Agugliaro, F., 2018. Mango stone properties as biofuel and its potential for reducing CO2 emissions. Journal of cleaner production 190, 53-62.

Phys.org, 2018. Spanish farmers go nuts for almonds as global demand booms. https://phys.org/news/2018-09-spanish-farmers-nuts-almonds-global.html accessed on 6th February 2019.

Queirós, C.S., Cardoso, S., Lourenço, A., Ferreira, J., Miranda, I., Lourenço, M.J.V., Pereira, H., 2019. Characterization of walnut, almond, and pine nut shells regarding chemical composition and extract composition. Biomass Conversion and Biorefinery, 1-14.

Sáez-Martínez, F.J., Lefebvre, G., Hernández, J.J., Clark, J.H., 2016. Drivers of sustainable cleaner production and sustainable energy options. Journal of Cleaner Production 138, 1-7.

Saghir, M., Naimi, Y., 2019. Energy Recovery from Waste in Fez city (Morocco), 2019 International Conference of Computer Science and Renewable Energies (ICCSRE). IEEE, pp. 1-6.

Scarlat, N., Dallemand, J.-F., Monforti-Ferrario, F., Nita, V., 2015. The role of biomass and bioenergy in a future bioeconomy: Policies and facts. Environmental Development 15, 3-34.

Schinke, B., Klawitter, J., Zejli, D., Barradi, T., Garcia, I., Leidreiter, A., 2016. Background Paper: Country Fact Sheet Morocco. Energy and Development at a Glance 2016, 58.

Schwanninger, M., Rodrigues, J., Pereira, H., Hinterstoisser, B., 2004. Effects of short-time vibratory ball milling on the shape of FT-IR spectra of wood and cellulose. Vibrational Spectroscopy 36(1), 23-40.

Segal, L., Creely, J., Martin Jr, A., Conrad, C., 1959. An empirical method for estimating the degree of crystallinity of native cellulose using the X-ray diffractometer. Textile Research Journal 29(10), 786-794.

Singh, Y.D., Mahanta, P., Bora, U., 2017. Comprehensive characterization of lignocellulosic biomass through proximate, ultimate and compositional analysis for bioenergy production. Renewable Energy 103, 490-500.

Smil, V., 2019. Energy in world history. Routledge.

Togibasa, O., Haryati, E., Dahlan, K., Ansanay, Y., Siregar, T., Liling, M., 2019. Characterization of Bio-battery from Tropical Almond Paste, Journal of Physics: Conference Series. IOP Publishing, p. 012036.

UN-SDG, 2019. Sustainable development goal 7. https://sustainabledevelopment.un.org/sdg7 accessed on 12/09/2019

Vassilev, S.V., Baxter, D., Andersen, L.K., Vassileva, C.G., 2010. An overview of the chemical composition of biomass. Fuel 89(5), 913-933.

Vassilev, S.V., Vassileva, C.G., Song, Y.-C., Li, W.-Y., Feng, J., 2017. Ash contents and ash-forming elements of biomass and their significance for solid biofuel combustion. Fuel 208, 377-409.

Vo, T.K., Ly, H.V., Lee, O.K., Lee, E.Y., Kim, C.H., Seo, J.-W., Kim, J., Kim, S.-S., 2017. Pyrolysis characteristics and kinetics of microalgal Aurantiochytrium sp. KRS101. Energy 118, 369-376.

Wang, J., Lian, W., Li, P., Zhang, Z., Yang, J., Hao, X., Huang, W., Guan, G., 2017. Simulation of pyrolysis in low rank coal particle by using DAEM kinetics model: Reaction behavior and heat transfer. Fuel 207, 126-135.

Wang, T., Hou, H., Ye, Y., Rong, H., Li, J., Xue, Y., 2019. Combustion behavior of refuse-derived fuel produced from sewage sludge and rice husk/wood sawdust using thermogravimetric and mass spectrometric analyses. Journal of Cleaner Production 222, 1-11.

Wang, T., Meng, D., Zhu, J., Chen, X., 2020. Effects of pelletizing conditions on the structure of rice straw-pellet pyrolysis char. Fuel 264, 116909.

Wang, X., Zhai, M., Wang, Z., Dong, P., Lv, W., Liu, R., 2018. Carbonization and combustion characteristics of palm fiber. Fuel 227, 21-26.

WorldBank, 2017. World Bank Group Announcements at One Planet Summit. https://www.worldbank.org/en/news/press-release/2017/12/12/world-bank-group-announcements-at-one-planet-summit accessed on 18th January 2019.

Wuebbles, D., Fahey, D., Hibbard, K., Dokken, D., Stewart, B., Maycock, T., 2017. US GLOBAL CHANGE RESEARCH PROGRAM CLIMATE SCIENCE SPECIAL REPORT (CSSR).

Xu, F., Shi, Y.-C., Wang, D., 2013. X-ray scattering studies of lignocellulosic biomass: a review. Carbohydrate polymers 94(2), 904-917.

Yin, C.-Y., 2011. Prediction of higher heating values of biomass from proximate and ultimate analyses. Fuel 90(3), 1128-1132.

Yu, D., Xu, M., Sui, J., Liu, X., Yu, Y., Cao, Q., 2005. Effect of coal particle size on the proximate composition and combustion properties. Thermochimica Acta 439(1-2), 103-109.

Zou, H., Evrendilek, F., Liu, J., Buyukada, M., 2019. Combustion behaviors of pileus and stipe parts of Lentinus edodes using thermogravimetric-mass spectrometry and Fourier transform infrared spectroscopy analyses: Thermal conversion, kinetic, thermodynamic, gas emission and optimization analyses. Bioresource technology 288, 121481.

Zu, S., Li, W.-z., Zhang, M., Li, Z., Wang, Z., Jameel, H., Chang, H.-m., 2014. Pretreatment of corn stover for sugar production using dilute hydrochloric acid followed by lime. Bioresource technology 152, 364-370.